AIAA 2000–4741

Two-dimensional High-Lift Aerodynamic Optimization Using the Continuous Adjoint Method

Sangho Kim, Juan J. Alonso and Antony Jameson
Stanford University, Stanford, CA 94305

8th AIAA/USAF/NASA/ISSMO Symposium on Multidisciplinary Analysis and Optimization September 6–8, 2000/Long Beach, CA

AIAA 2000–4741

Two-dimensional High-Lift Aerodynamic Optimization Using the Continuous Adjoint Method

Sangho Kim,* Juan J. Alonso† and Antony Jameson‡
Stanford University, Stanford, CA 94305

An adjoint-based Navier-Stokes design and optimization method for two-dimensional multi-element high-lift configurations is derived and presented. The compressible Reynolds-Averaged Navier-Stokes (RANS) equations are used as a flow model together with the Spalart-Allmaras turbulence model to account for high Reynolds number effects. Using a viscous continuous adjoint formulation, the necessary aerodynamic gradient information is obtained with large computational savings over traditional finite difference methods. A previous study of accuracy of the gradient information provided by the adjoint method, in comparison with finite differences and an inverse design of a single-element airfoil are also presented for validation of the present viscous adjoint method. The high-lift configuration design method uses a compressible Reynolds-Averaged Navier-Stokes (RANS) flow solver, FLO103-MB, a point-to-point matched multi-block grid system and the Message Passing Interface (MPI) parallel solution methodology for both the flow and adjoint calculations. Airfoil shape, element positioning, and angle of attack are used as design variables. The prediction of high-lift flows around a baseline three-element airfoil configuration, denoted as 30P30N, is validated by comparisons with experimental data. Finally, several design results that verify the effectiveness of the method for high-lift system design and optimization, are presented. Firstly, C_d is minimized and C_l is maximized for a single-element airfoil. Secondly, a multi-element inverse design problem is presented that attempts to match a pre-specified target pressure distribution using the shape of all elements in the airfoil, as well as their relative positions. Finally, the lift-to-drag ratio of a multi-element airfoil is maximized with fixed C_d or fixed C_l.

Introduction

THE motivation for this study is twofold: on the one hand, we would like to improve the take-off and landing performance of existing high-lift systems using an adjoint formulation. On the other hand, we would like to setup a numerical optimization procedure that can be useful to the aerodynamicist in the rapid design and development of high-lift system configurations and that can also provide derivative information regarding the influence of various design parameters (gap, overlap, slat and flap deflection angles, etc.) on the performance of the system.

The primary goal of an aerodynamic high-lift system is to increase payload capacity and reduce take-off and landing distances by increasing both the lift coefficient at a given angle of attack and the maximum lift coefficient. Traditionally, high-lift designs have been realized by careful wind tunnel testing which is both expensive and difficult due to the extremely complex flow interactions. Recently computational fluid dynamics (CFD) analyses have also been incorporated to the high-lift design process.[1] In particular, automatic design procedures, which use CFD combined with gradient-based optimization techniques, have made it possible to remove the difficulties in the decision making process (traditionally taken by a designer[2,3]). Generally, in gradient-based optimization techniques, a control function, which is to be optimized (an airfoil shape, for example), is parameterized using a set of design variables, and a suitable cost function to be minimized/maximized is defined (drag coefficient, lift/drag ratio, difference from a specified pressure distribution, etc). Then, the sensitivity derivatives of the cost function with respect to the design variables are calculated in order to get a direction of improvement. A step is taken in this direction and the procedure is repeated until convergence to a minimum is achieved. Finding a fast and accurate way of calculating the necessary gradient information is essential to developing an effective design method, since this may be the most time consuming portion of the design algorithm. A computationally efficient option, the control theory approach to optimal aerodynamic design in which gra-

*Doctoral Candidate, AIAA Member
†Assistant Professor, Department of Aeronautics and Astronautics , AIAA Member
‡Thomas V. Jones Professor of Engineering, Department of Aeronautics and Astronautics, AIAA Fellow

dient information is obtained via the solution of an adjoint equation, was first applied to transonic flow by Jameson[4–6] and has become a popular choice for design problems involving fluid flow.[7–10] The adjoint method is extremely efficient since the computational expense incurred in the calculation of the complete gradient with respect to an arbitrary number of design variables is effectively *independent* of the number of design variables. The only cost involved is the calculation of *one* flow solution and *one* adjoint solution whose complexity is similar to that of the flow solution. Aerodynamic design calculations using the Reynolds Averaged Navier-Stokes equations as the flow model have only recently been tackled by the authors.[11] The assessment of the accuracy of the gradient information that can be obtained from these adjoint equations and several design examples for a single-element airfoil have been presented in a previous paper.[11] In this study, the present viscous adjoint method is applied to high-lift system design in order to make use of the viscous design capability. Multi-element airfoils provide an additional challenge to the adjoint method: the effect of the changes in the shape of one element must be felt by the other elements in the system. Although preliminary information regarding the success of the adjoint method in such an environment is already available, the work in this paper will be used to validate this assumption. The design method, which is greatly accelerated by the use of control theory, can be further enhanced by the use of parallel computing. In this study a parallel implementation using a domain decomposition approach and the MPI standard for communication is used.[7,12]

Procedure

In this section we outline the overall design procedure used for a variety of design calculations that will be presented later. After the initial flowchart, each of the items of the procedure are explained in more detail. The overall design procedure can be summarized as follows:

1. Parameterize the configuration of interest using a set of design variables, and choose their values to define the initial configuration.

2. Solve the flow equations for ρ, u_1, u_2,u_3, p.

3. Solve the adjoint equations for the adjoint variable, ψ subject to appropriate boundary conditions.

4. Evaluate the gradient $\mathcal{G}$.

5. Update the shape based on the direction of steepest descent.

6. Return to 2.

Fig. 1 Definitions of Gap, Overlap, and Deflection Angles

Design Variables

The variables that describe the relative element positioning can be used as design variables. These variables include flap and slat deflection angles, gaps, and overlaps. The meaning of these variables can be easily seen in Figure 1 for typical multi-element airfoil configurations. For the present study, gaps and overlaps are used in an indirect way since the rigging is controlled by x and y directional translation of the slat and flap leading edges. In this way, the element positioning variables can be more easily changed independently each other. Needless to say, the actual values of overlaps and gaps can be easily recovered from their leading and trailing edge locations. The shapes of each of the elements are also used as design variables so as not to rule out the possibility that the optimum solution may be obtained with a combination of shape and position modifications. In fact, for the drag minimization of a single-element RAE2822 airfoil in transonic flow, the strong shock present at transonic flow conditions can only be eliminated using a small change in the shape of the airfoil. The coordinates of mesh nodes on the surface of the airfoil, Hick-Henne "*bump*" functions, patched polynomials and frequency based decompositions can be used to represent each of the elements in the high-lift system. For example, several of the following Hicks-Henne functions, which have been implemented and used for this study, are added to the baseline airfoil to modify the shape:

$$b\left(x\right) = A\left[\sin\left(\pi x^{\frac{\log 5}{\log t_1}}\right)\right]^{t_2}, \qquad 0 \leq x \leq 1.$$

Here, A is the maximum bump magnitude, t_1 locates the maximum of the bump at $x = t_1$, and t_2 controls

the width of the bump. Using this parameterization, two options are available for obtaining the optimum $C_{l_{max}}$. Firstly, $C_{l_{max}}$ can be predicted by maximizing C_l at a given angle of attack, then predicting the $C_{l_{max}}$ along a C_l vs. α line for that configuration, and repeating this procedure iteratively. Alternatively, $C_{l_{max}}$ may also be maximized directly by including angle of attack as a design variable in the optimization process.

Grid Topology

A multi-block mesh is generated prior to the iterative design loop so that the flow and adjoint equations can be suitably discretized. One-to-one point connectivity between block faces is employed to ensure conservation across boundaries and to provide for continuity of the grid at block interfaces. Once the initial grid is generated, new grids corresponding to modified airfoil shapes are obtained automatically during the design process by using an automatic mesh perturbation scheme (WARP-MB) that is essentially equivalent to shifting grid points along coordinate lines depending on the modifications to the shape of the boundary.

The modification to the grid has the form

$$x^{new} = x^{old} + \mathcal{N}\left(x^{new}_{airfoil} - x^{old}_{airfoil}\right)$$

$$y^{new} = y^{old} + \mathcal{N}\left(y^{new}_{airfoil} - y^{old}_{airfoil}\right).$$

Here,

$$\mathcal{N} = \frac{length_{total} - length_j}{length_{total}}.$$

The details of the procedure used have been presented earlier and can be found in Ref.[13,14]

Multi-block Flow and Adjoint Solvers

The prediction of high-lift flows poses a particularly difficult challenge for both CFD and turbulence modeling. Even in two-dimensions, the physics involved in the flow around a geometrically-complex high-lift device are quite sophisticated. In this study FLO103-MB, a multi-block RANS solver similar to the three-dimensional version of Reuther and Alonso,[8,15] is used for multi-element airfoil flow-field predictions. FLO103-MB satisfies the requirements of accuracy, convergence, and robustness that are necessary in this work. FLO103-MB solves the steady two-dimensional RANS equations using a modified explicit multistage Runge-Kutta time-stepping scheme. A finite volume technique and second order central differencing in space are applied to the integral form of the Navier-Stokes equations. The Jameson-Schmidt-Turkel(JST) scheme with adaptive coefficients for artificial dissipation is used to prevent odd-even oscillations and to allow for the clean capture of shock waves and contact discontinuities. In addition, local time stepping, implicit residual smoothing, and the multigrid method are applied to accelerate convergence to steady-state solutions. The Baldwin-Lomax algebraic model and the Spalart-Allmaras one equation model are used to model the Reynolds stress. The adjoint gradient accuracy study which was presented in a previous publication[11] was based on the Baldwin-Lomax model. This model is used for the single-element design cases of the present paper. Although this algebraic model has some advantages due to its implementational simplicity and robustness, the use of this model must be restricted to design at lower angles of attack and to the design of simpler geometries such as single-element airfoils. For actual high-lift designs such as $C_{l_{max}}$ maximization, the one-equation Spalart-Allmaras model is used for better predictions of both the $C_{l_{max}}$ and the flow physics around complex geometries.[16–18] The turbulent equation is solved separately from the flow equations using an alternating direction implicit (ADI) method. The turbulence equation is updated at the start of each multistage Runge-Kutta time step on the finest grid of the multigrid cycle only. The adjoint solution is obtained with the exact same numerical techniques used for the flow solution. The implementation exactly mirrors the flow solution modules inside FLO103-MB, except for the boundary conditions which are imposed on the co-state variables.

Continuous Adjoint Method

For the flow about an airfoil or wing, the aerodynamic properties which define the cost function are usually functions of the flow-field variables, w, and the physical location of the boundary, which may be represented by the function $\mathcal{F}$. Then

$$I = I\left(w, \mathcal{F}\right),$$

and a change in $\mathcal{F}$ results in a change

$$\delta I = \frac{\partial I^T}{\partial w}\delta w + \frac{\partial I^T}{\partial \mathcal{F}}\delta \mathcal{F}, \tag{1}$$

in the cost function. Using control theory, the governing equations of the flow field are introduced as a constraint in such a way that the final expression for the gradient does not require reevaluation of the flow field. In order to achieve this δw must be eliminated from (1). Suppose that the governing equation R which expresses the dependence of w and $\mathcal{F}$ within the flow field domain D can be written as

$$R\left(w, \mathcal{F}\right) = 0. \tag{2}$$

Then δw is determined from the equation

$$\delta R = \left[\frac{\partial R}{\partial w}\right]\delta w + \left[\frac{\partial R}{\partial \mathcal{F}}\right]\delta \mathcal{F} = 0. \tag{3}$$

Next, introducing a Lagrange Multiplier ψ, we have

$$\begin{aligned}\delta I &= \frac{\partial I^T}{\partial w}\delta w + \frac{\partial I^T}{\partial \mathcal{F}}\delta \mathcal{F} - \psi^T\left(\left[\frac{\partial R}{\partial w}\right]\delta w + \left[\frac{\partial R}{\partial \mathcal{F}}\right]\delta \mathcal{F}\right) \\ &= \left\{\frac{\partial I^T}{\partial w} - \psi^T\left[\frac{\partial R}{\partial w}\right]\right\}\delta w + \left\{\frac{\partial I^T}{\partial \mathcal{F}} - \psi^T\left[\frac{\partial R}{\partial \mathcal{F}}\right]\right\}\delta \mathcal{F}.\end{aligned}$$

Choosing ψ to satisfy the adjoint equation

$$\left[\frac{\partial R}{\partial w}\right]^T \psi = \frac{\partial I}{\partial w} \tag{4}$$

the first term is eliminated, and we find that

$$\delta I = \mathcal{G}\delta\mathcal{F}, \tag{5}$$

where

$$\mathcal{G} = \frac{\partial I^T}{\partial \mathcal{F}} - \psi^T \left[\frac{\partial R}{\partial \mathcal{F}}\right].$$

The advantage is that (5) is independent of δw, with the result that the gradient of I with respect to an arbitrary number of design variables can be determined without the need for additional flow-field evaluations. In the case that (2) is a partial differential equation, the adjoint equation (4) is also a partial differential equation and appropriate boundary conditions must be determined. The formulation of the adjoint equation and the boundary conditions are described in greater detail in previous publications[19] and a detailed gradient accuracy study for the continuous adjoint method can be found in Ref.[11]

Numerical Optimization Method

The search procedure used in this work is a simple steepest descent method in which small steps are taken in the negative gradient direction.

$$\delta\mathcal{F} = -\lambda\mathcal{G},$$

where λ is positive and small enough that the first variation is an accurate estimate of δI. Then

$$\delta I = -\lambda\mathcal{G}^T\mathcal{G} < 0.$$

After making such a modification, the gradient can be recalculated and the process repeated to follow a path of steepest descent until a minimum is reached.

Results

Validation of the Adjoint Method for Viscous Flows

This section presents the results of a gradient accuracy study for the RANS equations using the Baldwin-Lomax turbulence model, as well as a simple example of the use of the resulting gradient information in single-element airfoil inverse design. Gradient accuracy is assessed by comparison with finite-difference gradients and by examination of the changes in the magnitude of the gradients for different levels of flow solver convergence. For inverse design, the aerodynamic cost function chosen is given by:

$$I = \frac{1}{2}\int_{\mathcal{B}} (p - p_d)^2 \, dS, \tag{6}$$

which is simply the Euclidean norm of the difference between the current pressure distribution and a desired target, p_d, at a constant angle of attack, α. The gradient of the above cost function is obtained with respect to variations in 50 Hicks-Henne sine "bump" functions centered at various locations along the upper and lower surfaces of a baseline airfoil. The locations of these geometry perturbations are ordered sequentially such that they start at the lower surface of the trailing edge, proceed forward to the leading edge, and then back around to the upper surface of the trailing edge. Figure 2 shows a comparison between the most accurate gradients obtained using both the adjoint and finite-difference methods. There is a general agreement on all trends that validates the implementation of the present adjoint method. As mentioned in Section 2, the fundamental advantage is restated here that the gradient with respect to an arbitrary number of design variables, 50 for this example, is determined with the cost of only a single flow field evaluation and a single adjoint evaluation for any given design cycle.

Figure 3 shows the computed adjoint gradients for different levels of flow solver convergence. For Navier-Stokes calculations, the adjoint information is essentially unchanged if the level of convergence in the flow solver is at least 4 orders of magnitude. This is an additional advantage of using the adjoint method especially for the design of high-lift configurations for which it is difficult to obtain levels of convergence much higher than 4 orders of magnitude. This is in contrast with the high levels of convergence required for accurate sensitivity information when using the finite difference method. In viscous flows it is typical to require that the flow solver converge to about 6 orders of magnitude so that the gradient information is sufficiently accurate.

An inverse design problem which starts with an RAE2822 airfoil geometry and tries to obtain the shape that generates the pressure distribution around a NACA 64A410 airfoil at the same flow conditions is presented here. The mesh used for this Navier-Stokes calculation is a C-mesh with 512×64 cells. The target pressure specified is that of a NACA 64A410 airfoil at $M = 0.75$ and $\alpha = 0.0$. The Reynolds number of this calculation was set at $Re = 6.5$ million. Figure 4 shows the progress of the inverse design calculation. In 100 design iterations, the target pressure was matched almost exactly, including the correct strength and position of the shock. The initial RAE2822 airfoil geometry was altered to obtain a shape that is quite close to the NACA 64A410 airfoil that had produced the target pressure distribution in the first place. The norm of the pressure error was reduced from 0.0504 to 0.0029 in 100 design iterations.

FLO103-MB With SA Model Validation

Flow convergence

Figure 5 shows the convergence history of the averaged density residual for the calculation of the flow field around the 30P30N high-lift configuration using

the flow solver, FLO103-MB. The Spalart-Allmaras one equation turbulence model is used for this calculation. The solution converges down to somewhere in the range of 10^{-4} and 10^{-5} in about 2000 iterations. Although small oscillations remains after 2000 iterations, the C_l, one of the cost functions used for subsequent designs, has converged without oscillations. As mentioned earlier in Section 2, this level of convergence is also good enough to get accurate sensitivity information using the adjoint method.

Comparisons with Experimental Data

Results of the comparisons between computational results and experimental data are presented below for validation purposes. These examples are limited to a single multi-element airfoil configuration for lack of space. The code, FLO103-MB, and the solver it derives from, TFLO, have been extensively validated for a variety of test cases, ranging from flat plates to transonic axisymmetric bumps, to full three-dimensional configurations.

Figure 6, shows the comparison of the computational and experimental C_p distributions around the 30P30N configuration at $M = 0.2$, $\alpha = 8.0$, and Re$= 9M$. The agreement between experimental and computational distributions is very encouraging. Integrated pressure coefficients also agree quite well.

In order to validate the ability of the flow solver to predict stall using the SA turbulence model, a comparison of C_l versus angle of attack is shown in Figure 7. The total coefficient of lift together with the lift from the three components is plotted in the range of $-5 < \alpha < 25$. The computed results agree quite well with experiment with slightly higher predictions of $C_{l_{max}}$ and angle of attack at $C_{l_{max}}$. Although the results do not agree with experiment exactly, it has been observed that the choice of turbulence model can have a substantial impact on the numerical values of some of these parameters. The stall prediction capability can be a critical factor for actual design cases, such as $C_{l_{max}}$ maximization. Without the use of the SA turbulence model, these quantities can be overpredicted substantially.

Finally, for further validation, velocity profiles from both computation and from experiment are compared at two different locations on the main element and the flap. Streamwise velocity components are plotted against normal distance to the wall at $x/c = 0.45$, which lies on the main element and at $x/c = 0.89817$, which is directly on the flap. The computed velocity profiles predict well both the velocity gradient in the boundary layer and gradients due to the wakes of the slat and main element. Good agreement between computational and experimental data is therefore observed.

Single-Element Airfoil Design

The variety of designs presented in this subsection were all carried out using a 4 block multiblock mesh with a total number of cells equal to 512×64. The Baldwin-Lomax turbulence model was used in all test cases. The four designs presented had as a starting point the RAE2822 airfoil, and computations were carried out at a Reynolds number of 6.5 million. The surface of the airfoil was parameterized using 50 Hicks-Henne bump functions, 25 of which are distributed evenly along the upper surface of the airfoil, while the remaining 25 are placed in a similar fashion along the lower surface.

C_d Minimization at a Fixed Angle of Attack

Figure 9 shows the result of a typical viscous design calculation where the total coefficient of drag of the airfoil is minimized using a parameterization with 50 design variables. The design calculation is carried out without changing the angle of attack of the airfoil, which does not guarantee that the coefficient of lift will be maintained. It is clear from the figure that the optimization procedure has changed the geometry in such a way that the initial strong shock wave has completely disappeared. The coefficient of drag of the airfoil has dropped from 0.0152 to 0.0100, while the C_l undergoes only a small reduction. Most of the drag reduction in this test case comes from the elimination of the wave drag.

C_d Minimization at a Fixed C_l

This test case is similar to the previous one, except for the fact that the optimization procedure is forced to achieve a near constant C_l. This constraint is achieved by periodically adjusting the angle of attack during the flow solution portion of the design procedure. Figure 10 shows the result of 50 design iterations for this test case. As in the case of constant angle of attack, the optimizer is able to eliminate the strong shock wave that existed in the initial design by using the values of the same 50 design variables. The modifications to the geometry are slightly more dramatic. Once the design process is completed, the total coefficient of drag has been reduced from 0.0167 to 0.0109, while, if anything, the C_l has only increased slightly from 0.8243 to 0.8305. Notice that the final pressure distribution is quite similar to that obtained in the previous test case.

C_l Maximization at a Fixed Angle of Attack

In this test case, we attempt to maximize the C_l of the RAE2822 airfoil by altering its shape using the same 50 Hicks-Henne design functions and without changing the angle of attack of the configuration. Interestingly, the optimizer proceeds to almost completely eliminate the strong shock on the upper surface, thus allowing itself to carry a larger amount of lift. The lift coefficient increases from 0.7991 to 0.8566

in only 18 design iterations, while the C_d is considerably reduced from 0.0152 to 0.0109. Figure 11 shows the results of this test case. Notice that the character of the resulting pressure distribution is very similar to that obtained in the drag minimization test cases but with a more pronounced suction peak and a mild shock on the upper surface.

C_l Maximization at a Fixed C_d

Finally, if we constrain the coefficient of drag to be constant, more interesting results can be found. Figure 12 shows the result of this type of design optimization. The front portion of the upper surface of the configuration is modified considerably to produce a very different pressure distribution that allows for the existence of a shock wave on the upper surface that considerably increases the amount of lift carried by the airfoil. In addition, since the C_d is constrained to be constant (this is imposed by allowing the angle of attack to float), the resulting angle of attack is also higher, again leading to the creation of a higher lift coefficient.

Multi-Element Airfoil Design

Except for the inviscid test cases presented in the first subsection below, all of the results in this section were computed using a multiblock viscous meshes constructed using either a C- or an O-topology. The C-topology mesh, for example, has 28 blocks of varying sizes and a total of 162,816 cells. The O-mesh is of similar size. All calculations are carried out at a free stream Mach number, $M = 0.20$ and a Reynolds number, Re$= 9 \times 10^6$. The computation of the Reynolds stress is carried out using the Spalart-Allmaras turbulence model.

Apart from the first inviscid test case, the results in this section mimic those in the single-element airfoil section as far the design procedure is concerned. Comparison between the results of single- and multi-element optimizations are left to the reader.

Inverse Design Using the Euler Equations

In order to verify the implementation of our design procedure, we present a simple test case first which is aimed at verifying that the multiblock flow and adjoint solvers are capable of producing correct sensitivities to both shape modifications and rigging variables in a multi-element airfoil design environment. For this purpose, an inviscid grid around the 30P30N configuration was constructed. A perturbed geometry was created by activating a single bump on the upper surface of the main element and by deflecting the flap by an increment of 2°. The pressure distribution around the original geometry is used as a target pressure distribution (seen as a solid line in Figure 13) for the perturbed geometry to arrive at through an inverse design process. Notice that the modification of the geometry described above influences the pressure distribution in all three elements: slat, main, and flap.

A total of 156 design variables are used to parameterize the complete configuration. 50 bump functions are used in each of the three elements. In addition, both the slat and the flap are allowed to translate in the x and y directions and to rotate about their leading edges. After 100 design iterations where sensitivities with respect to all design variables were calculated, the target pressure distribution is recovered as expected. The original geometry is also recovered. The results of this inviscid test case provide the necessary confidence to tackle some of the more complex viscous cases we present below.

C_d Minimization at a Fixed Angle of Attack

In this test case, the 30P30N airfoil is analyzed at an angle of attack $\alpha = 16.02$. The result of this analysis is taken as the baseline, and without changing the angle of attack, we attempt to minimize the total drag coefficient of the configuration. Notice that, as opposed to the single-element test case, the Mach number of the flow is subsonic throughout and, therefore, no shock waves are present. Since the design procedure is unable to eliminate the inexistent wave drag, it must focus on viscous and profile drag. By slightly reshaping the main element and by repositioning the flap, the C_d decreases from 0.0834 to 0.0795. All of this reduction in C_d is not attributed to the optimizer, since the lift has also decreased from 4.0747 to 3.9966 in the three design iterations presented here.

C_l Maximization at a Fixed Angle of Attack

A similar calculation to the one presented above is discussed in this section. Instead of minimizing C_d, however, we maximize the C_l of the configuration using all 156 design variables in the problem. As before, the angle of attack of the whole configuration remains constant, $\alpha = 8.01$. Once again, the restriction on variations in angle of attack of the whole configuration is too strong, and the optimizer is only able to make minor improvements in C_l after 5 design iterations: the lift coefficient has increased from 3.1514 to 3.1698. Notice that this small increase in lift has also delivered a decrease in drag, contrary to expectations. The C_d decreases from 0.0651 to 0.0647 in the same 5 design iterations.

C_l Maximization at a Fixed C_d

Finally, we attempt to allow the angle of attack to float by fixing the value of the C_d to that of the baseline design point at $\alpha = 15.855$. As we can see in Figure 16, in 5 design iterations, the optimizer has increased the lift by a small amount (from 3.8986 to 3.9113) while reducing both the angle of attack and the total coefficient of drag. This result appears counterintuitive at first but highlights the power of both the adjoint methodology and the careful parameterization of the surface, since the procedure still yields a

higher C_l, while the angle of attack is forced down to match the prescribed C_d.

Conclusions

A numerical optimization procedure using the adjoint method for high-lift system design has been developed and presented. The procedure is based on a multiblock RANS flow solver that has been named FLO103-MB that uses the Spalart-Allmaras turbulence model for high Reynolds number flows. FLO103-MB has been implemented in parallel so that the turnaround for design calculations can be even faster.

Multi-element airfoils are parameterized using the well-known Hicks-Henne bump functions and additional design variables that allow the gaps and overhangs, as well as the angle of attack setting of the slat and flap elements to be represented. Making use of the large computational savings provided by the adjoint method when large numbers of design variables are involved, we are able to explore high-dimensional design spaces that are necessary for high-lift system design. In this study, the 30P30N multi-element airfoil is used because experimental data is available for validation purposes. A total of 156 design variables corresponding to 50 Hicks-Henne bump functions on each of the elements of the configuration, and the x and y locations and the angles of attack of the slat and flap elements are used.

After a brief discussion on the accuracy of gradient information resulting from the proposed viscous adjoint methodology, results for C_l maximization and C_d minimization for a single-element airfoil are presented. Similar test cases are shown for the 30P30N multi-element airfoil. The results obtained are encouraging and point out that the adjoint method can have great potential for the design of high-lift systems. However, further research is needed to clarify some aspects of C_l maximization problems where the angle of attack of the configuration is allowed to vary, especially, close to the stall angle for a given configuration. The stall point is particularly troublesome since the force coefficients, which are assumed to behave smoothly, may present discontinuities there.

Future work will focus on expanding the results of the current paper and on utilizing the method described above to perform realistic two-dimensional high-lift system designs.

Acknowledgments

This research has been made possible by the generous support of the David and Lucille Packard Foundation in the form of a Stanford University School of Engineering Terman fellowship. The solution of the Spalart-Allmaras turbulence model is an adaptation of Dr. Creigh McNeil's implementation embedded in the three-dimensional version of our flow solver. Thanks also go to Dr. Kuo-Cheng of the Boeing Company for providing us with the multi-element airfoil experimental data. Finally, the authors acknowledge the assistance of Kaveh Hosseini in the post-processing of the multiblock data in this work.

References

[1]S. X. Ying. High lift chanllenges and directions for cfd. Technical report, AIAA/NPU AFM Conference Proceedings, China, June 1996.

[2]S. Eyi, K. D. Lee, S. E. Rogers, and D. Kwak. High-lift design optimization using navier-stokes equations. *Journal of Aircraft*, 33:499–504, 1996.

[3]Eric Besnard, Adeline Schmitz, Erwan Boscher, Nicolas Garcia, and Tuncer Cebeci. Two-dimensional aircraft high lift system design and optimization. *AIAA paper 98-0123*, 1998.

[4]A. Jameson. Aerodynamic design via control theory. *Journal of Scientific Computing*, 3:233–260, 1988.

[5]A. Jameson. Optimum aerodynamic design using CFD and control theory. *AIAA paper 95-1729*, AIAA 12th Computational Fluid Dynamics Conference, San Diego, CA, June 1995.

[6]A. Jameson. Re-engineering the design process through computation. *AIAA paper 97-0641*, 35th Aerospace Sciences Meeting and Exhibit, Reno, Nevada, January 1997.

[7]J. Reuther, J.J. Alonso, M.J. Rimlinger, and A. Jameson. Aerodynamic shape optimization of supersonic aircraft configurations via an adjoint formulation on parallel computers. *AIAA paper 96-4045*, 6th AIAA/NASA/ISSMO Symposium on Multidisciplinary Analysis and Optimization, Bellevue, WA, September 1996.

[8]J. Reuther, J. J. Alonso, J. C. Vassberg, A. Jameson, and L. Martinelli. An efficient multiblock method for aerodynamic analysis and design on distributed memory systems. *AIAA paper 97-1893*, June 1997.

[9]O. Baysal and M. E. Eleshaky. Aerodynamic design optimization using sensitivity analysis and computational fluid dynamics. *AIAA paper 91-0471*, 29th Aerospace Sciences Meeting, Reno, Nevada, January 1991.

[10]W. K. Anderson and V. Venkatakrishnan. Aerodynamic design optimization on unstructured grids with a continuous adjoint formulation. *AIAA paper 97-0643*, 35th Aerospace Sciences Meeting and Exhibit, Reno, Nevada, January 1997.

[11]S. Kim, J. J. Alonso, and A. Jameson. A gradient accuracy study for the adjoint-based navier-stokes design method. *AIAA paper 99-0299*, AIAA 37th Aerospace Sciences Meeting & Exhibit, Reno, NV, January 1999.

[12]J. Reuther, A. Jameson, J. J. Alonso, M. J. Rimlinger, and D. Saunders. Constrained multipoint aerodynamic shape optimization using an adjoint formulation and parallel computers. *AIAA paper 97-0103*, 35th Aerospace Sciences Meeting and Exhibit, Reno, Nevada, January 1997.

[13]J. J. Reuther, A. Jameson, J. J. Alonso, M. Rimlinger, and D. Saunders. Constrained multipoint aerodynamic shape optimization using an adjoint formulation and parallel computers: Part I. *Journal of Aircraft*, 36(1):51–60, 1999.

[14]J. J. Reuther, A. Jameson, J. J. Alonso, M. Rimlinger, and D. Saunders. Constrained multipoint aerodynamic shape optimization using an adjoint formulation and parallel computers: Part II. *Journal of Aircraft*, 36(1):61–74, 1999.

[15]L. Martinelli and A. Jameson. Validation of a multigrid method for the Reynolds averaged equations. *AIAA paper 88-0414*, 1988.

[16]P. R. Spalart and S. R. Allmaras. A one-equation turbulence model for aerodynamic flows. *AIAA paper 92-0439*, AIAA 30nd Aerospace Sciences Meeting & Exhibit, Reno, NV, January 1992.

[17]Christopher L. Rumsey, Thomas B. Gatski, Susan X. Ying, and Arild Bertelrud. Prediction of high-lift flows using turbulent closure models. *AIAA Journal*, 36:765–774, 1998.

[18]S. E. Rogers, F. R. Menter, and P. A. Durbin Nagi N. Mansour. A comparison of turbulence models in computing multi-element airfoil flows. *AIAA paper 94-0291*, AIAA 32nd Aerospace Sciences Meeting & Exhibit, Reno, NV, January 1994.

[19]A. Jameson, L. Martinelli, and N. A. Pierce. Optimum aerodynamic design using the Navier-Stokes equations. *Theoretical and Computational Fluid Dynamics*, 10:213–237, 1998.

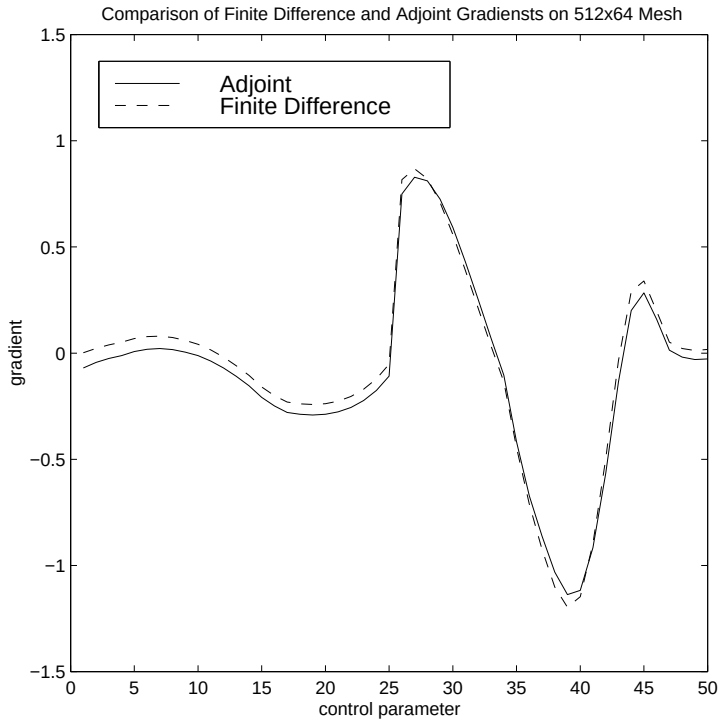

Fig. 2 Navier-Stokes Inverse Design: Comparison of Finite Difference and Adjoint Gradients for a 514x65 Mesh.

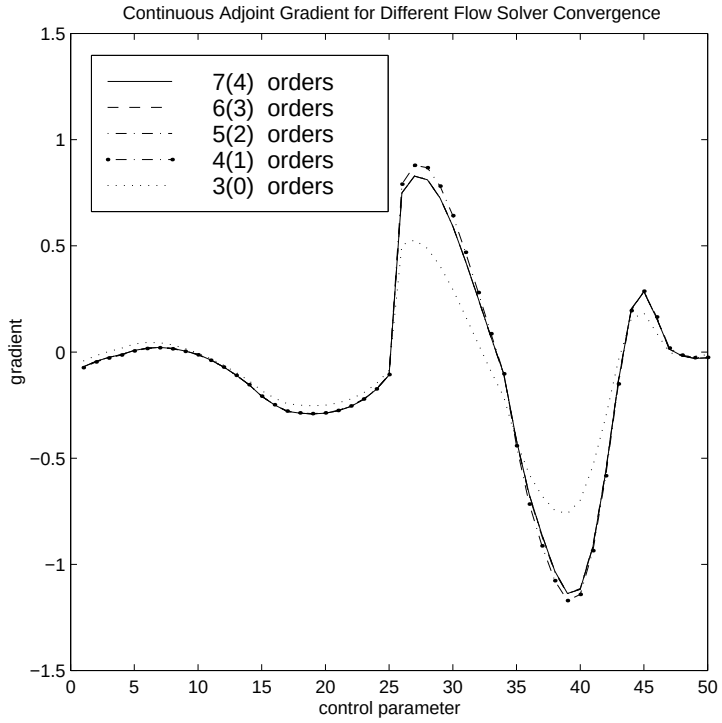

Fig. 3 Navier-Stokes Inverse Design: Adjoint Gradients for Varying Levels of Flow Solver Convergence.

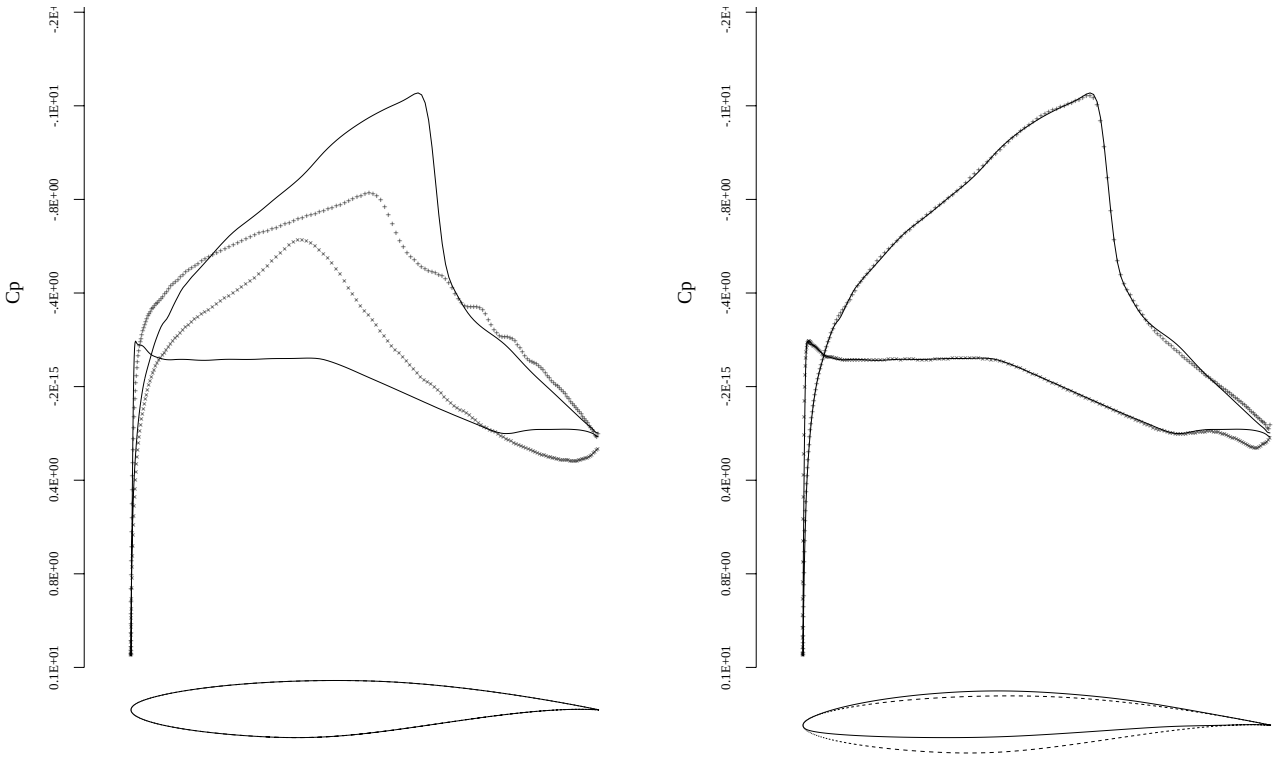

a) Initial, $P_{error} = 0.0504$ **b)** 100 Design Iterations, $P_{error} = 0.0029$

Fig. 4 Typical Navier-Stokes Inverse Design Calculation, RAE 2822 airfoil to NACA 64A410, $M = 0.75$**,** $\alpha = 0.0$**, Re =** 6.5 **million.**

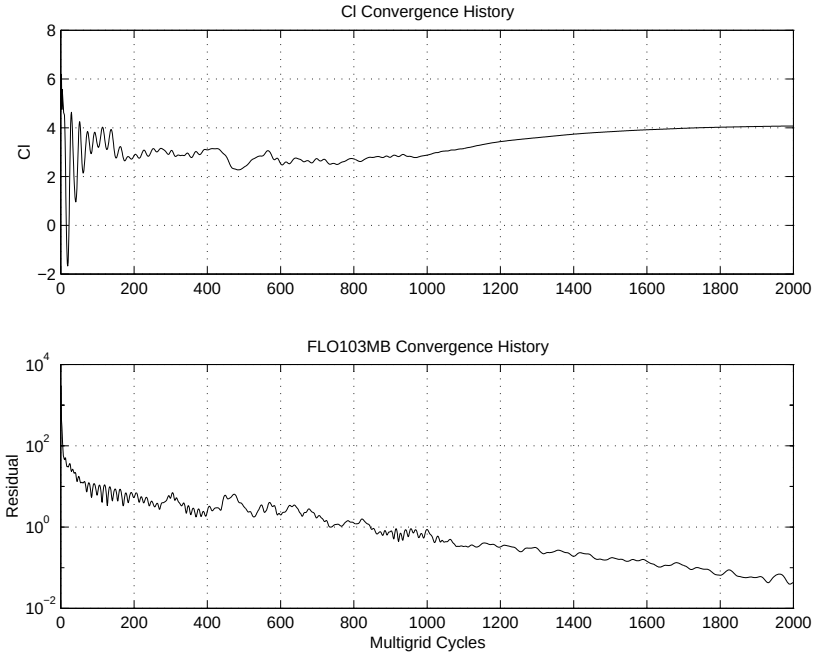

Fig. 5 Convergence History of C_l **and Density Residual for a Multi-Element Airfoil using the Spalart-Allmaras Turbulence Model.**

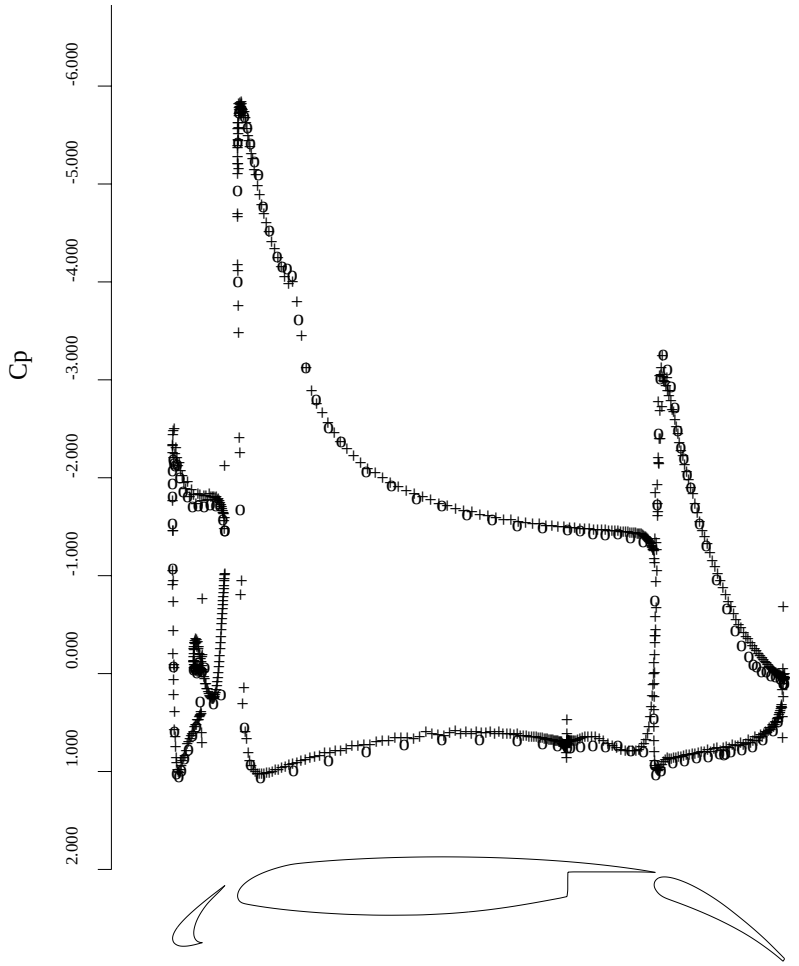

Fig. 6 Comparison of Experimental and Computational Pressure Coeffient Distributions for the 30P-30N Multi-element Airfoil.

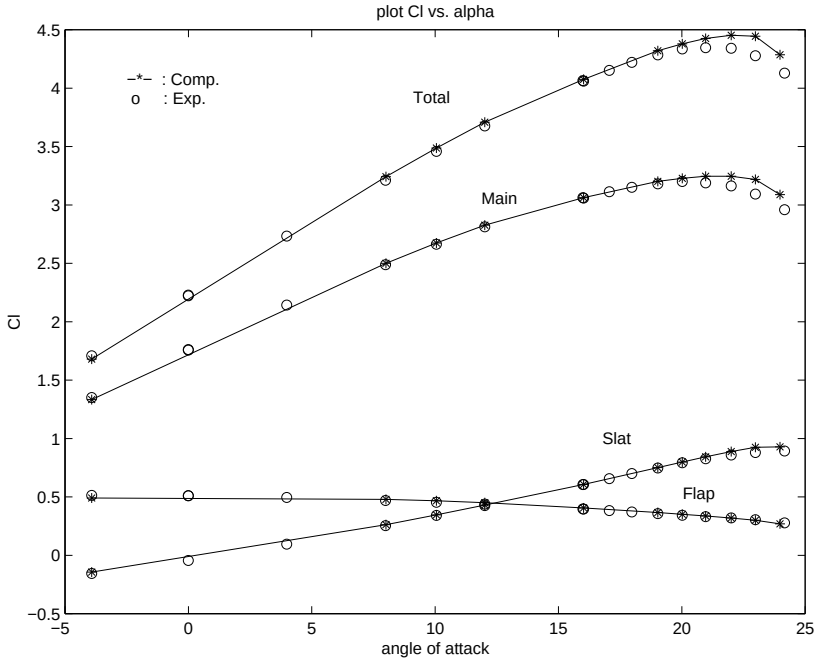

Fig. 7 Experimental and computational lift versus angle of attack comparison.

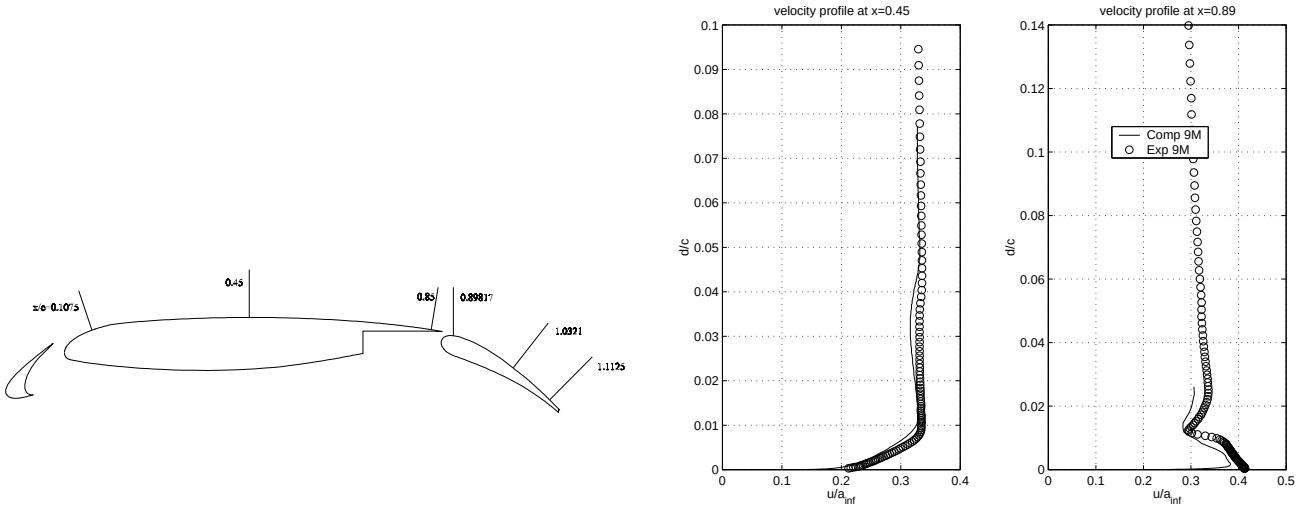

a) Location of Experimental Velocity Profiles.

b) Velocity profiles at x/c=0.45 and x/c=0.89817

Fig. 8 Comparison Between Computational and Experimental Velocity Profiles, $M = 0.20$**,** $\alpha = 8.0$**,** $Re = 9$ **million.**

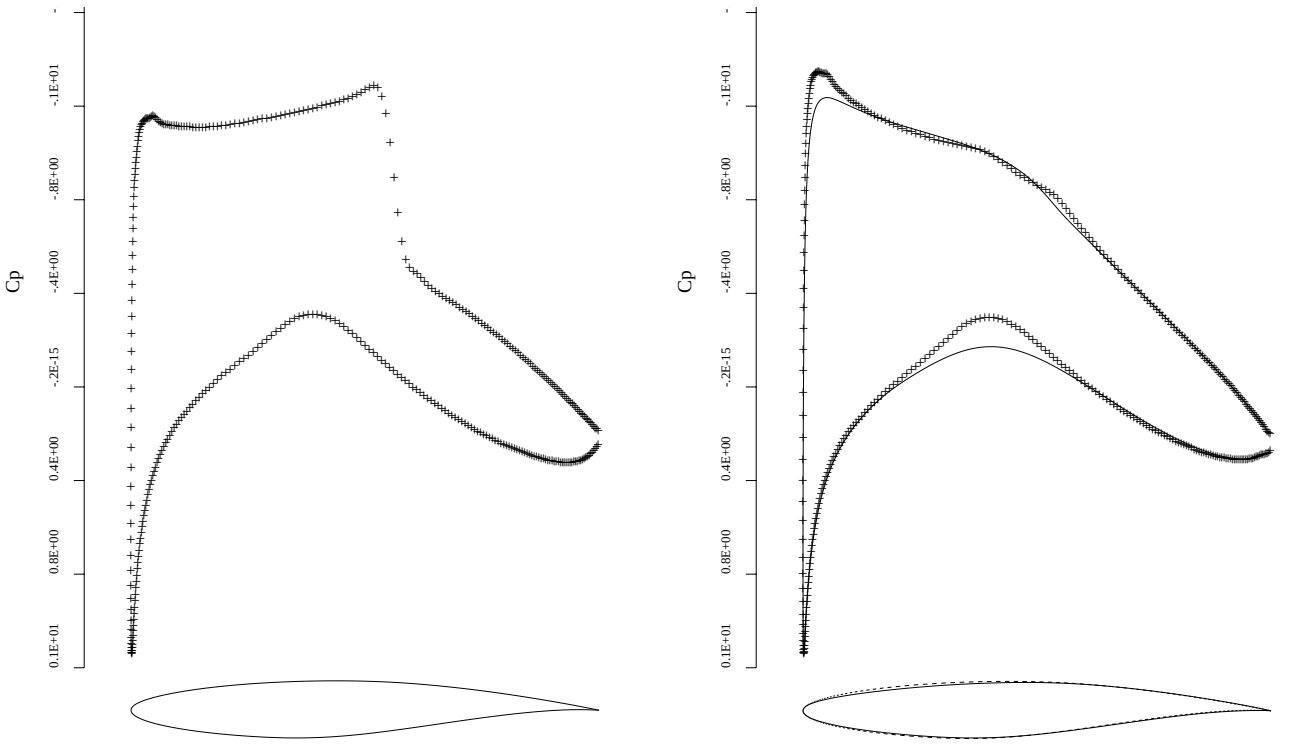

a) Initial, $CD = 0.0152$, $M = 0.73$, α=2.79, $CL = 0.7991$

b) 15 Design Iterations,$CD = 0.0100$, $M = 0.73$, α=2.79, $CL = 0.7814$

Fig. 9 Typical Navier-Stokes Drag Minimization Calculation at Fixed α**=2.79, RAE 2822 Airfoil**

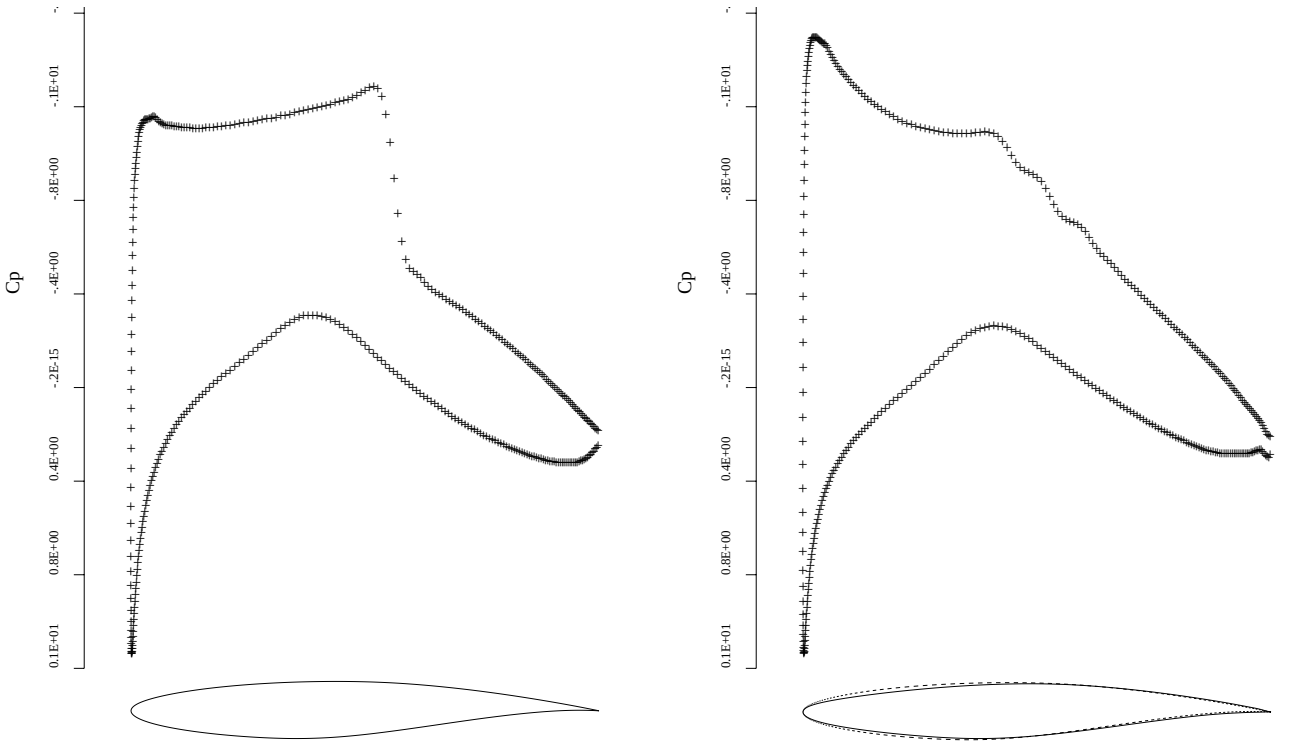

a) Initial, $CD = 0.0167$, $M = 0.73$, α=2.977, $CL = 0.8243$

b) 50 Design Iterations,$CD = 0.0109$, $M = 0.73$, α=3.172, $CL = 0.8305$

Fig. 10 Typical Navier-Stokes Drag Minimization Calculation at Fixed $CL = 0.83$, RAE 2822 Airfoil

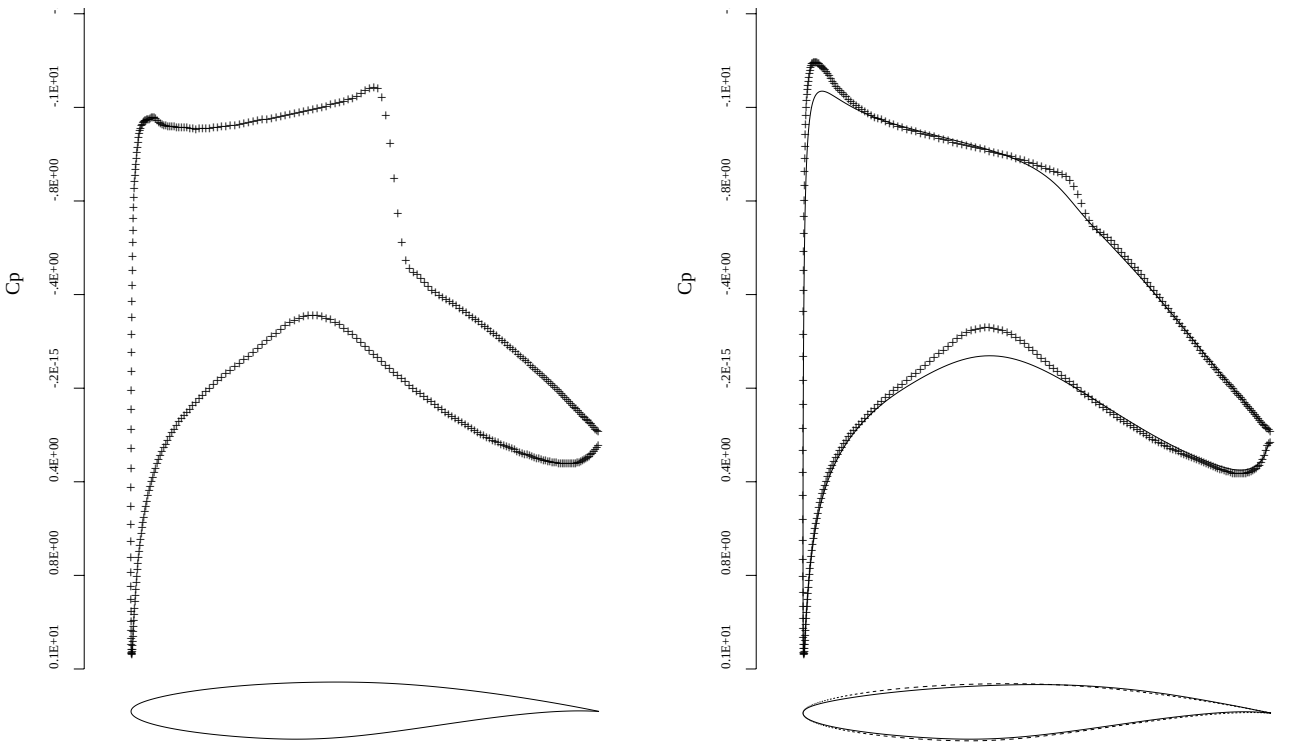

a) Initial, $CL = 0.7991$, $M = 0.73$, $\alpha = 2.79$, $CD = 0.0152$

b) 18 Design Iterations,$CL = 0.8566$, $M = 0.73$, α=2.79, $CD = 0.0109$

Fig. 11 Typical Navier-Stokes Lift Maximization Calculation at Fixed $\alpha = 2.79$, RAE 2822 Airfoil

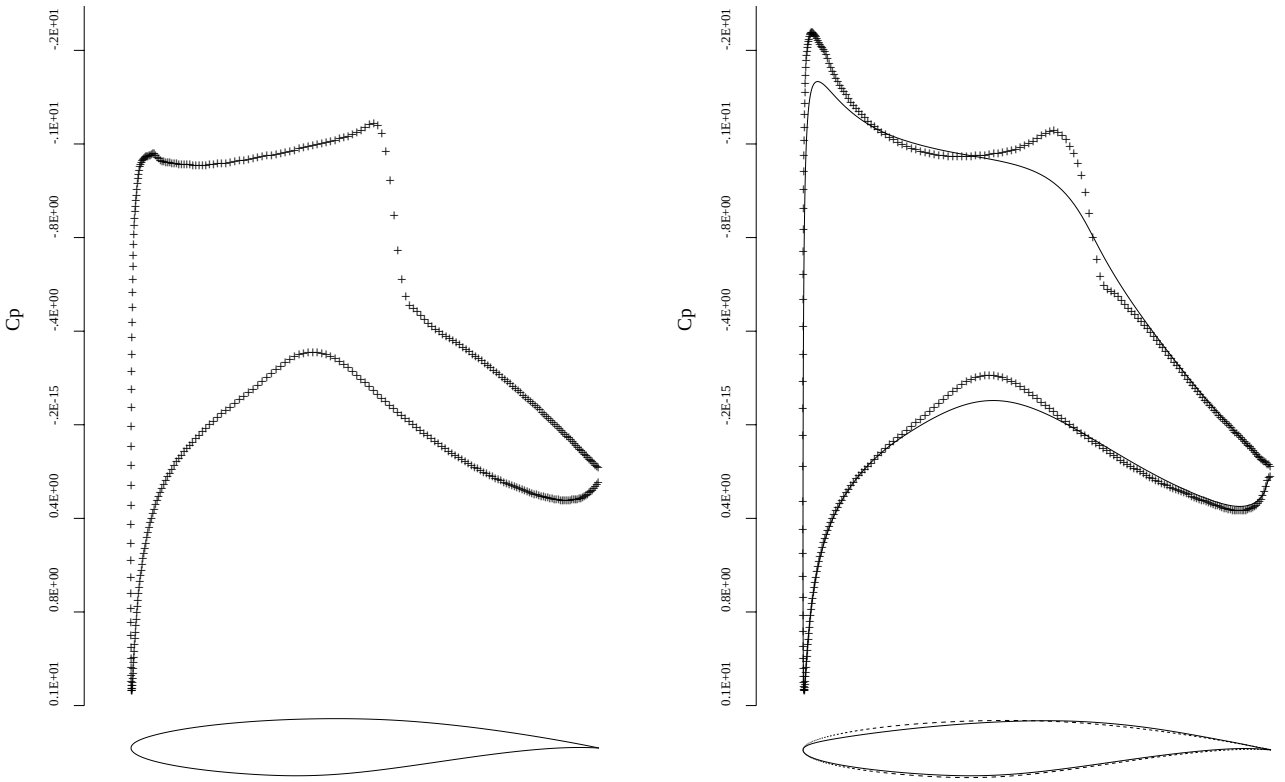

a) Initial, $CL = 0.7991$, $M = 0.73$, $\alpha = 2.796$, $CD = 0.0153$

b) 18 Design Iterations,$CL = 0.9761$, $M = 0.73$, $\alpha = 3.375$, $CD = 0.0153$

Fig. 12 Typical Navier-Stokes Lift Maximization Calculation at Fixed $CD = 0.0153$, RAE 2822 Airfoil

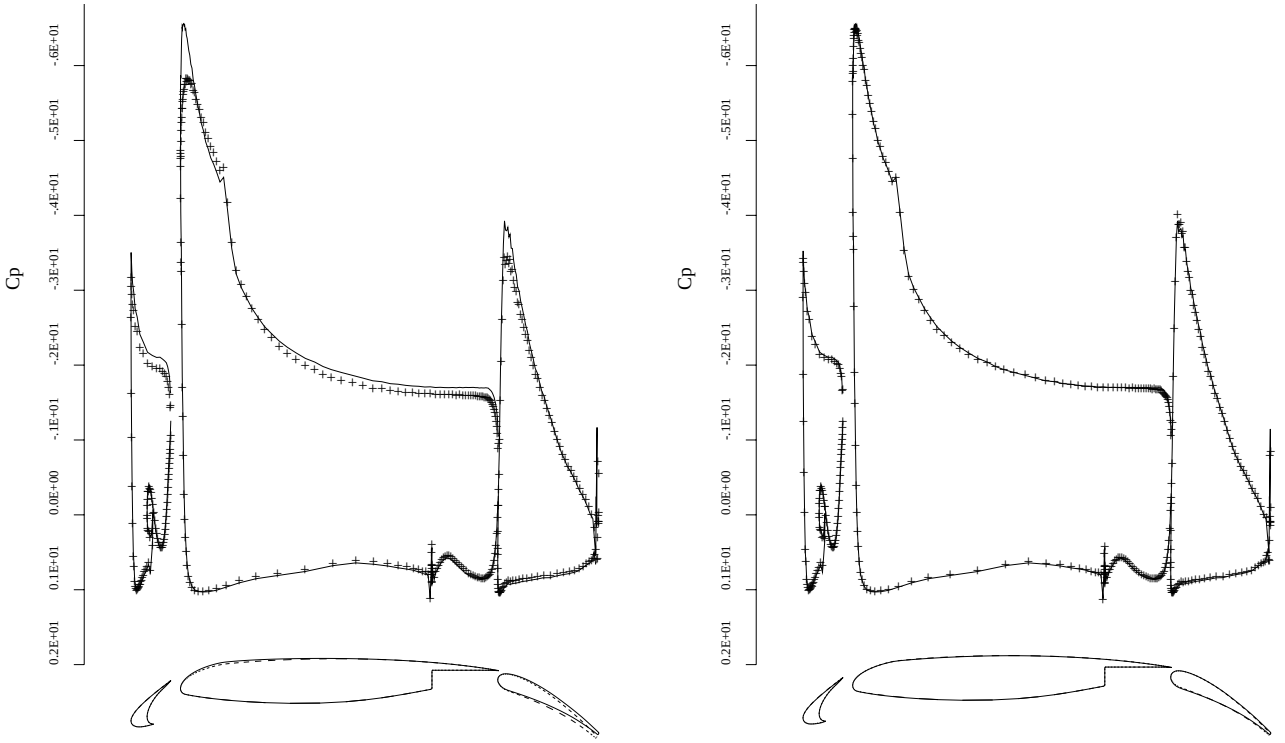

a) Initial Geometry with One Bump on the Main Element and a 2° Deflection on the Flap

b) 100 Design Iterations Using All Bumps and Rigging Variables

Fig. 13 Example of Multi-Element Euler Inverse Design

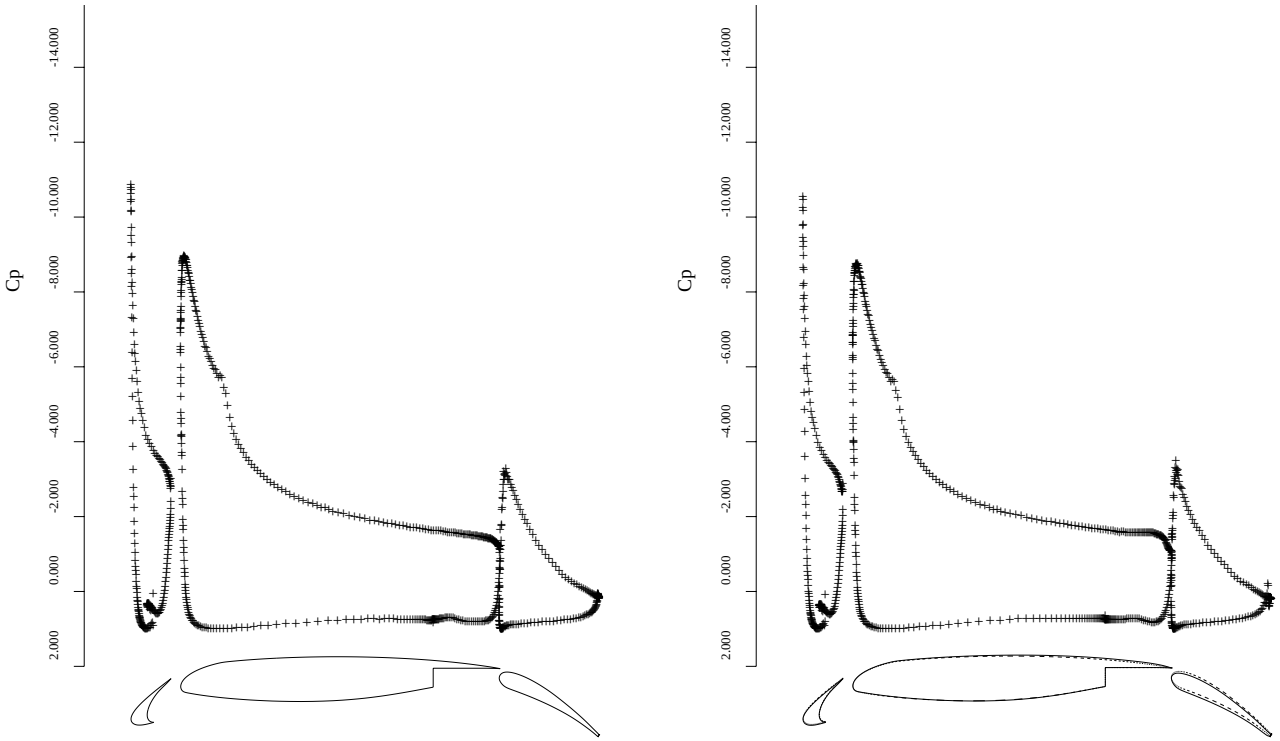

a) Initial, $CD = 0.0834$, $M = 0.2$, α=16.02, $CL = 4.0747$

b) 3 Design Iterations,$CD = 0.0795$, $M = 0.2$, α=16.02, $CL = 3.9966$

Fig. 14 Multi-Element Airfoil Drag Minimization Calculation at Fixed α=16.02, 30P30N

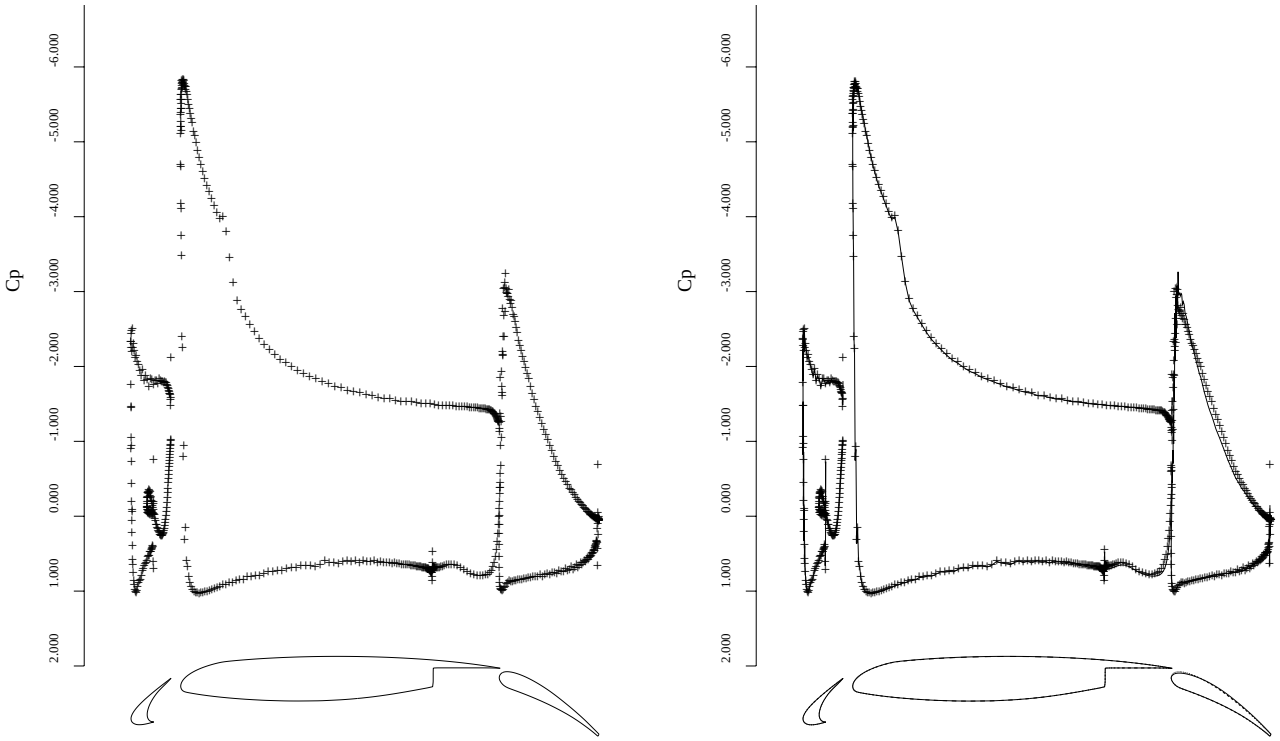

a) Initial, $CL = 3.1514$, $M = 0.2$, $\alpha = 8.01$, $CD = 0.0651$

b) 5 Design Iterations,$CL = 3.1698$, $M = 0.2$, α=8.01, $CD = 0.0647$

Fig. 15 Multi-Element Airfoil Lift Maximization Calculation at Fixed α=8.01, 30P30N

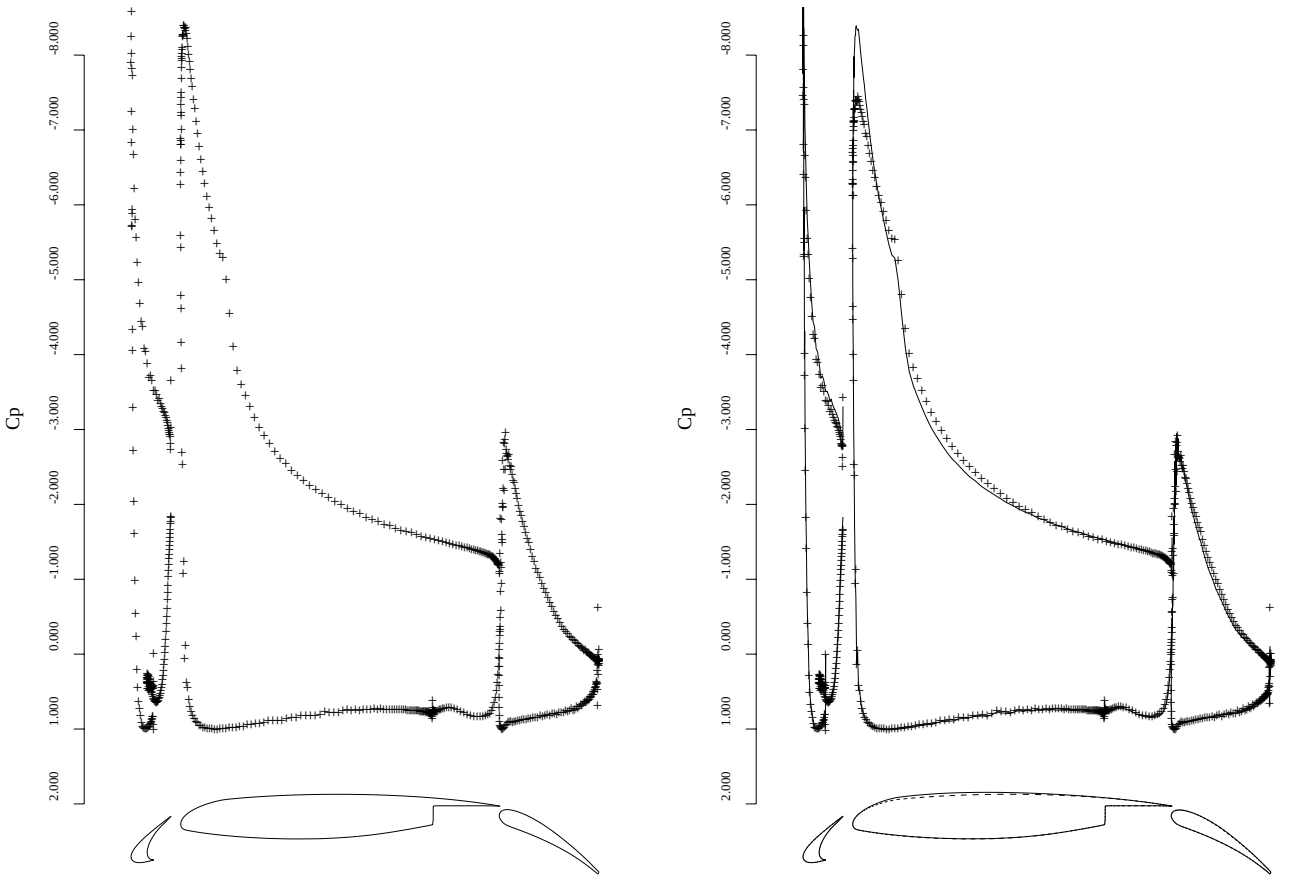

a) Initial, $CL = 3.8986$, $M = 0.2$, $\alpha = 15.855$, $CD = 0.0898$

b) 5 Design Iterations,$CL = 3.9113$, $M = 0.2$, $\alpha = 15.281$, $CD = 0.0875$

Fig. 16 Multi-Element Airfoil Lift Maximization Calculation at Fixed $CD = 0.083$, 30P30N